



LAWRENCE  
LIVERMORE  
NATIONAL  
LABORATORY

# Land-Atmosphere Coupling Manifested in Warm-Season Observations on the U.S. Southern Great Plains

T. J. Phillips, S. A. Klein

June 28, 2013

Journal of Geophysical Research - Atmospheres

## **Disclaimer**

---

This document was prepared as an account of work sponsored by an agency of the United States government. Neither the United States government nor Lawrence Livermore National Security, LLC, nor any of their employees makes any warranty, expressed or implied, or assumes any legal liability or responsibility for the accuracy, completeness, or usefulness of any information, apparatus, product, or process disclosed, or represents that its use would not infringe privately owned rights. Reference herein to any specific commercial product, process, or service by trade name, trademark, manufacturer, or otherwise does not necessarily constitute or imply its endorsement, recommendation, or favoring by the United States government or Lawrence Livermore National Security, LLC. The views and opinions of authors expressed herein do not necessarily state or reflect those of the United States government or Lawrence Livermore National Security, LLC, and shall not be used for advertising or product endorsement purposes.

Land-Atmosphere Coupling Manifested in Warm-Season  
Observations on the U.S. Southern Great Plains

Thomas J. Phillips and Stephen A. Klein  
Lawrence Livermore National Laboratory  
Livermore, California 94551

Revised Submission for *Journal of Geophysical Research-Atmospheres*

January 8, 2014

## **Abstract**

This study examines several observational aspects of land-atmosphere coupling on daily average time scales during warm seasons of the years 1997 to 2008 at the Department of Energy Atmospheric Radiation Measurement Program's Southern Great Plains (SGP) Central Facility site near Lamont, Oklahoma. Characteristics of the local land-atmosphere coupling are inferred by analyzing the covariability of selected land and atmospheric variables that include precipitation and soil moisture, surface air temperature, relative humidity, radiant and turbulent fluxes, as well as low-level cloud base height and fractional coverage. For both the energetic and hydrological aspects of this coupling, it is found that large-scale atmospheric forcings predominate, with local feedbacks of the land on the atmosphere being comparatively small much of the time. The weak land feedbacks are manifested by 1) the inability of soil moisture to comprehensively impact the coupled land-atmosphere energetics, and 2) the limited recycling of local surface moisture under conditions where most of the rainfall derives from convective cells that originate at remote locations. There is some evidence, nevertheless, of the local land feedback becoming stronger as the soil dries out in the aftermath of precipitation events, or on days when the local boundary-layer clouds are influenced by thermal updrafts known to be associated with convection originating at the surface. Potential implications of these results for climate-model representation of regional land-atmosphere coupling also are discussed.

## 1. Introduction

Land-atmosphere coupling, as manifested in both models and observations, has received increasing scientific attention during the past decade (e.g. see the review by Seneviratne et al. [2010]). Pioneering studies of this type were initially conducted with individual climate models (e.g. see the summary by Dirmeyer et al. [2012] ), but broader scientific attention was sparked by the first Global Land-Atmosphere Coupling Experiment (GLACE-1) performed by twelve general circulation models (GCMs) [Koster et al., 2004, 2006]. The participating models individually displayed diverse behaviors in their coupling of simulated soil moisture with surface air temperature, and especially precipitation, over many regions during boreal summer [Guo et al., 2006]. Nonetheless, several semi-arid transitional regions characterized by persistent soil moisture stress were identified, where the strength of this land-atmosphere coupling was relatively large in a multimodel, ensemble-mean sense. The implication was that seasonal prediction of precipitation, in particular, could be improved from knowledge of soil moisture near these regional “hot spots”, one of which was located in the central U.S.

Initial diagnosis of land-atmosphere coupling in the GLACE-1 models focused mainly on the response of terrestrial turbulent fluxes (especially evapotranspiration) to soil-moisture anomalies. Subsequent analysis (e.g. Guo et al. [2006], Santanello et al. [2011a]) emphasized that substantial soil moisture-precipitation feedback also requires a strong linkage between the surface fluxes and precipitation that is usually mediated by locally triggered convection.

To estimate large-scale surface flux-convection linkages, Findell et al. [2011], Ferguson and Wood [2011], and Taylor et al. [2012] have followed alternative approaches, employing North American Regional Reanalysis (NARR) moist products that reflect assimilation of observed precipitation (Findell et al. [2011]), or various satellite-derived products (Ferguson and Wood [2011] and Taylor et al. [2012]). The Findell et al. [2011] study also differed in scope, in that it

considered only the relationship between surface evaporation and convective potential, whereas Ferguson and Wood [2011] and Taylor et al. [2012] also accounted for effects of satellite-estimated soil moisture. While not in close agreement with one another, results of these analyses implied that the central U.S. is not a “hot spot” for locally initiated convective precipitation compared with other parts of North America (especially the southeast U.S.). In addition, Taylor et al. [2012] questioned whether coarse-resolution climate models were inherently capable of properly representing surface-induced mesoscale flows thought to be important in triggering convection over land. An extensive satellite-based study conducted by Ferguson et al. [2012] also suggested that models of various kinds (e.g. off-line land models forced by observations as well as global and NARR atmospheric reanalysis models coupled to land models) generally overestimate the coupling strength of soil moisture, surface evaporative flux, and boundary-layer lifting condensation level (LCL). Nevertheless, Ferguson et al. [2012] confirmed that the GLACE-identified, semi-arid transitional zones were indeed sites of *relatively strong* land-atmosphere coupling.

While such studies provide useful estimates of large-scale variations in land-atmosphere coupling, they remain subject to the limitations of relatively coarse-scale remote sensing and model-based reanalysis products. To complement these large-scale investigations, it is desirable to exploit *in-situ* observations at locations where these are available. For example, the U.S. Department of Energy (USDOE) Southern Great Plains (SGP) network of field sites, are arranged in a roughly 3.5x3.5-degree area about a Central Facility (CF) that is located (at 36.6 N, 97.5 W) near Lamont, Oklahoma. Here extensive high-frequency observing systems have operated continuously since the mid-1990s under the USDOE Atmospheric Radiation Measurement (ARM) Program [Ackerman and Stokes, 2003; Mather and Voyles, 2013].

The ARM SGP data streams thus afford unique opportunities for conducting analyses of local land-atmosphere interactions in this central-U.S. region that are of particular scientific interest. In the aftermath of the GLACE-1 modeling experiment, several studies of this type have been undertaken. Dirmeyer et al. [2006] used ARM SGP data (among others) to compare soil moisture-atmosphere coupling in the GLACE-1 climate models with equivalent observables. They highlighted substantial deficiencies in GLACE model simulations of the local observed relationships among soil moisture, surface turbulent fluxes, and precipitation. Lamb et al. [2012] combined SGP field data in May-June periods during four years with North American Regional Reanalysis (NARR) atmospheric wind and moisture products in order to study the components of the regional moisture budget centered on SGP. They estimated the daily average moisture recycling fraction for the SGP region to be small, ranging only between 0.07-0.28. Most recently, Ruiz-Barradas and Nigam [2013] employed pentadal ARM SGP observations supplementing NARR products to analyze the relative roles played by horizontal and vertical moisture transports in determining regional precipitation variability. They found that horizontal moisture transports dominated, consistent with a relatively small amount of local precipitation recycling. This result confirmed their earlier assertion that GLACE-vintage models exhibited overly strong vertical moisture transports in compensating for too weak horizontal transports over the central U.S. [Ruiz-Barradas and Nigam, 2006].

Taken together, these SGP regional studies would appear to call into question the GLACE-1 model ensemble mean result implying the presence of a tight land-atmosphere hydrological coupling over the central U.S. It thus is desirable to bring additional in-situ observational data to bear on this problem, and to consider their consistency with previous SGP regional studies of this type. The recent release of ARM Best Estimate (ARMBE) quality-controlled data sets provides

such an opportunity for more detailed studies of land-atmosphere coupling in this region [Xie et al., 2010]. At the SGP CF site, for example, the ARMBE data comprise measurements of many diverse surface and atmospheric variables taken at hourly intervals over a 12-year period.

It is the goal of the present study to exploit the ARMBE data for a more comprehensive investigation of land-atmosphere coupling (including interactions among soil moisture, surface radiative and turbulent fluxes, low-level clouds, and precipitation), and over a longer period than has previously been attempted at the SGP CF site. Moreover, the wide range of available ARMBE-observed variables permits quantification of the relative strengths of feedbacks between land and atmosphere.

The analysis approach is mainly inspired by the perspectives of Alan Betts [e.g. Betts et al., 1996, Betts, 2004 and Betts, 2009] which have influenced many of the aforementioned land-atmosphere studies. In Betts' framework, the atmosphere forces the land via radiant fluxes and precipitation that are modulated by clouds, while the land feeds back on the atmosphere via radiant and turbulent fluxes that are modulated by soil moisture. These interactions usually are depicted as scatter plots expressing the covariation of selected land surface and atmospheric variables.

This study thus seeks to identify multiple examples of the covariation of diverse observed surface and lower-atmospheric variables that are indicative of several aspects of the local land-atmosphere coupling particular to the SGP CF site. The analysis focuses on daily average quantities (constructed from hourly ARMBE observations) for the May-August warm seasons of the years 1997-2008, when land-atmosphere coupling is likely to be strongest. The ARMBE data are augmented, as needed, by a few auxiliary ARM data sets, and this study is also informed by

investigations of ARM-observed SGP clouds and precipitation conducted by Zhang and Klein [2010, 2013].

The ARMBE data characteristics and the analysis methodology are discussed further in Section 2. Details of the observed SGP land-atmosphere energetic and hydrological interactions are presented in Sections 3 and 4, respectively. The implications of the study are elaborated in Section 5, and ideas for future investigations of land-atmosphere coupling that would combine observations with model experiments are offered in a concluding Section 6.

## **2. Data Characteristics and Analysis Approach**

The ARM data archive holdings are vast and exceptionally diverse in terms of observed variables, instruments, measurement frequencies; it thus can be challenging for the uninitiated user to efficiently access relevant data. To make these data more accessible to climate model developers and diagnosticians in particular, ARM Best Estimate (ARMBE) data sets have been assembled [Xie et al., 2010]. The ARMBE data at SGP are presently only provided for the CF site. These data consist of hourly samples over the course of multiple years, presently from 1997 to 2008 for most variables. (Less comprehensive data measured at other ARM sites such as those on the North Slope of Alaska and at several locations in the Western Equatorial Pacific also are available over shorter time periods.)

At SGP CF, the ARMBE data include vertical soundings of state variables, a variety of cloud characteristics (e.g. vertical cloud fraction and total cloud cover, liquid water path, etc.), surface downward and upward radiant fluxes, sensible and latent heat fluxes, precipitable water, and surface meteorology such as winds, temperature, relative humidity. For the current study, however, only a subset of the available ARMBE variables are considered, while several additional quantities are obtained from other ARM data holdings (see Table 1). Rough estimates

of the respective instrumental root-mean-square measurement error (RMSE), gleaned from the cited references in Table 1, also are listed. For instance, the error in measuring the surface sensible heat flux is larger than that for the surface radiant fluxes, due to the propagation of errors from measurements of the net surface radiation, wind, surface temperature, relative humidity, and soil moisture that are required for estimation of this flux.

In the results to be described in Sections 3 and 4, the correlation between selected pairs of land surface and atmospheric variables during the May-August warm seasons are displayed as scatter plots, reflecting diverse aspects of the land-atmosphere coupling. Following Betts' emphasis, the focus of the present study is on *daily average* quantities, which are computed from hourly data between the hours of 0 Z to 23 Z, or roughly from local early evening to late afternoon of the following day. For many variables, the daily averages appear to be quite insensitive to the choice of temporal endpoints but, for physical reasons, the averaging of certain variables in Table 1 (the surface shortwave fluxes  $SW_{dn}$ ,  $SW_{dn\ clr}$ ,  $SW_{up}$  and albedos, as well as precipitation and the cloud base level CBL, for selected conditions) is done only over daytime hours from 12 Z to 23 Z.

Because of intermittent instrument failures, some hourly data were missing from the ARMBE and ancillary products, and so the daily averaging algorithm needed to take such missing values into account. When an entire day of observations was missing for a variable, no daily average was computed. For those time intervals where  $M < 24$  hourly samples per day were available for a given variable, the  $M$  samples were summed, and the resulting value was then divided by  $M$  to yield a pseudo-daily average. While some sampling bias may have been introduced in such cases, this was viewed as preferable to completely disregarding days with only a few hours of missing data. (Most daily averages included at least 16 hourly samples.)

To assess the relative coherence of different aspects of land-atmosphere coupling, a quantitative measure of the coherence of the covariation of variables  $y$  and  $x$ , such as the temporal correlation coefficient, is needed:

$$R = \langle x'y' \rangle / (\sigma_x \sigma_y) \quad (1)$$

Here  $x'$  and  $y'$  signify the departures of each sampled variable from its multi-year statistical mean (with their multi-year average product denoted by the angle brackets), while  $\sigma_x$  and  $\sigma_y$  are the corresponding standard deviations.

In order to assess the statistical significance of  $R$ , the number of independent samples  $N$  of  $y$  versus  $x$  must be estimated, taking account of missing data. There are a maximum total of 1476 daily average samples in the entire 1997-2008 time series but, for certain variables with considerable missing data (e.g. the surface turbulent fluxes  $H$  and  $LE$ ), only about 1100 daily averages enter into the calculation of correlation  $R$ . However, even such reduced numbers of samples are serially correlated, and hence are not statistically independent. If it is assumed [following Dirmeyer et al, 2012] that only one in every five daily averages can be treated as statistically independent, then there are approximately  $N = 220$  independent samples in a time series of 1100 daily averages. Applying a standard test for the statistical significance of a correlation  $R$  resulting from  $N = 220$  independent samples [e.g. Bulmer, 1979],  $|R| > 0.20$  can conservatively be regarded as statistically significant at a 99-% confidence level. (*Hereafter, a 99-% confidence level applies to all bivariate correlations described as “statistically significant”, unless explicitly stated otherwise.*) It should be kept in mind, of course, that a statistically significant correlation does not necessarily imply the existence of a causal relationship [e.g. Orłowsky and Seneviratne, 2010].

Because the  $R$  statistic can be sensitive to mismatches in the observed ranges of the  $x$  and  $y$  variables, Dirmeyer [2011] recommends use of a supplemental “sensitivity index”  $I$  defined as

$$I = \sigma_x \gamma \quad (2)$$

where  $\gamma$  is the slope of the least-squares regression line calculated from the scatter plot of  $y$  vs.  $x$ .  $I$  thus measures the magnitude of the average variation in  $y$  for a one-sigma variation in  $x$ . Since  $I$  takes on the units of  $y$ , this metric is most useful for comparing the sensitivities of different  $y$  variables, which are expressed in the same units, to variations in a common  $x$  variable (e.g. see Table 2). Values of both  $R$  and  $I$  thus are listed in the scatter plots that are shown.

### 3. Atmosphere-Land Energy Interactions Mediated by Clouds

This section presents salient aspects of land-atmosphere energetics. The approach involves considering relationships among the radiant fluxes and clouds, and then examining the response of the land surface to the radiant forcings, as evinced by the surface turbulent fluxes.

#### 3.1 Surface Radiant Fluxes

For given surface downward and upward short-wave fluxes  $SW_{\text{dn}}$  and  $SW_{\text{up}}$ , the net absorbed short-wave radiation at the surface is

$$SW_{\text{net}} = SW_{\text{dn}} - SW_{\text{up}} = (1 - \alpha_s) SW_{\text{dn}} \quad (3)$$

where the surface albedo  $\alpha_s$  is defined as the ratio  $SW_{\text{up}}/SW_{\text{dn}}$ . The slope  $\gamma$  of the least-squares regression line of 1997-2008 May-August hourly values of  $SW_{\text{up}}$  vs  $SW_{\text{dn}}$  (figure not shown) provides an estimated surface albedo  $\alpha_s$  of approximately 0.19. The correlation of hourly  $SW_{\text{up}}$  vs  $SW_{\text{dn}}$  is very high ( $R = 0.99$ ), as is to be expected on physical grounds. The sensitivity index  $I$ , calculated as the product of the regression slope and the standard deviation of independent variable  $SW_{\text{dn}}$  ( $\sigma_x = 331.99$ ), is correspondingly large ( $I = 64.64$ ).

For clear-sky (cloudless) conditions, the net surface short-wave radiation  $SW_{net}$  achieves a maximum value of  $(1 - \alpha_s)SW_{dn\ clr}$ . Here  $SW_{dn\ clr}$  is equivalent to the diurnal top-of-atmosphere downward short-wave insolation  $SW_{dn\ TOA}$  that is attenuated only by absorbing gases and aerosols in the atmospheric column over the SGP Central Facility. Observationally based hourly estimates of  $SW_{dn\ clr}$  after Long and Shi [2006] also are accessible from the ARM data archive for the years 1997-2008.

Most of the time, of course, the surface downward short-wave flux is less than its clear-sky value, due to reflection or absorption by clouds. To quantify their bulk radiant effects, it is useful to define an effective short-wave cloud albedo  $\alpha_c$  following Betts [2004, 2009]:

$$\alpha_c = (SW_{dn\ clr} - SW_{dn}) / SW_{dn\ clr} \quad (4)$$

The net short-wave radiation absorbed at the surface under cloudy conditions then can be expressed as

$$SW_{net} = (1 - \alpha_c) (1 - \alpha_s) SW_{dn\ clr} \quad (5)$$

During the warm season at SGP,  $\alpha_s$  is nearly constant and  $SW_{dn\ clr}$  changes only slowly, so (5) implies that  $SW_{net}$  will decrease quasi-linearly with increasing  $\alpha_c$ . This is mostly what is observed, but with outliers occurring, especially for values of  $\alpha_c$  less than about 0.4 (Figure 1a). The daily-average net total (net short-wave + net long-wave) radiant flux  $R_{net}$  varies similarly, although less coherently, with  $\alpha_c$  (Figure 1b). The correlation coefficient is correspondingly reduced in absolute value ( $R = -0.55$ ) from that in Figure 1a ( $R = -0.65$ ), and the sensitivity coefficients ( $I = -54.17$  and  $-37.36$ , respectively) change in a roughly consistent way.

The surface net longwave radiative flux  $LW_{net} = LW_{dn} - LW_{up}$  also plays an important role in the land-atmosphere energetic coupling. While both  $LW_{dn}$  and  $LW_{up}$  are temperature-sensitive,  $LW_{net}$  on daily-mean timescales also is strongly influenced by relative humidity and cloud cover, due to substantial vertical coupling of the atmosphere's diurnal temperature and moisture structure [Betts, 2009]. For instance, the highly positive correlations of the net surface longwave flux  $LW_{net}$  with  $\alpha_c$ , and with the surface relative humidity  $RH$ , are shown in Figure 2. (The positive correlation of  $LW_{net}$  with  $\alpha_c$  seen in Figure 2a is obscured in the analogous plot of net surface radiation  $R_{net}$  vs  $\alpha_c$  shown in Figure 1b, since  $SW_{net}$  predominates over  $LW_{net}$  in its contribution to  $R_{net}$ .)

$RH$  also covaries strongly with the effective shortwave cloud albedo  $\alpha_c$  ( $R = 0.61$ ,  $I = 0.13$ , figure not shown), since atmospheric relative humidity at cloud level is likely to be correlated somewhat, on daily-mean time scales, with its value at the surface. This relationship implies that the surface moisture might impact cloud horizontal extent or vertical thickness and, by extension, the surface shortwave energetics. Of course,  $RH$  is not solely a function of local surface conditions, but is also greatly influenced by moisture advection (e.g. from the Gulf of Mexico) on many warm-season days at the SGP site [Zhang and Klein, 2010].

### 3.2 Surface Turbulent Fluxes

In addition to the net total radiation  $R_{net}$ , the surface energy budget includes turbulent fluxes of latent and sensible heat  $LE$  and  $H$ , as well as the residual ground heat flux  $G$  which impacts the soil heat storage:

$$R_{net} = LE + H + G \quad (6)$$

Like  $R_{net}$  (Figure 1b),  $LE$  and  $H$  both vary inversely with effective cloud albedo  $\alpha_c$  (e.g. see the scatter plot for  $L$  in Figure 3a); but at SGP,  $LE$  covaries more strongly with  $\alpha_c$  ( $R = -0.38$ ,  $I = -22.13$ ) than does  $H$  ( $R = -0.29$ ,  $I = -10.35$ , figure not shown). For the daily average values of interest in this study,  $G$  is usually small relative to other components in (6), so that  $R_{net}$  is approximately balanced by the sum of the turbulent fluxes:

$$R_{net} \sim LE + H \quad (7)$$

For a given value of  $R_{net}$ ,  $LE$  and  $H$  thus display a rough “zero-sum” relationship with one another, and the correlation of  $H$  with  $(LE - R_{net})$  is thus found to be relatively large in absolute value ( $R = -0.82$  in Figure 3b). Where there is still substantial scatter about the regression line in Figure 3b, this signifies either that the ground flux  $G$  is sometimes sizeable, or that measurements of radiative and turbulent fluxes by different instruments exhibit perceptible errors.

Because the surface radiant and turbulent fluxes are expressed in the same units ( $\text{W m}^{-2}$ ) their sensitivity indices  $I$  with respect to the effective cloud albedo  $\alpha_c$  may be directly compared (Table 2). The index  $I$  imparts somewhat different information than does the correlation coefficient  $R$ , in that  $I$  is proportional to the slope of the regression line of variable  $y$  vs.  $x$  (change in  $y$  for a one-sigma change in  $x$ --cf. equation 2), while  $R$  is a measure of their coherence (dependent on the amount of scatter about the regression line). For example, the surface net shortwave  $SW_{net}$  and net total radiation  $R_{net}$  are seen to be considerably more sensitive to changes in effective cloud albedo  $\alpha_c$  ( $I = -54.17$  and  $-37.76$ , respectively) than is the net longwave flux  $LW_{net}$  ( $I = 14.88$ ) even though its correlation with  $\alpha_c$  is relatively large ( $R = 0.71$ ). The turbulent fluxes  $LE$  and  $H$  also are found to be relatively insensitive to changes in

effective cloud albedo ( $I = -22.13$  and  $-10.35$ , respectively), presumably because they are also impacted by surface properties, whose effects are next considered.

#### **4. Atmosphere-Land Interactions Mediated by Soil Moisture**

Aspects of atmosphere-land coupling evinced by related surface and lower-atmospheric moist processes are next considered. These include interactions among precipitation, soil moisture, evapotranspiration, relative humidity, and boundary-layer clouds at the SGP CF site.

##### **4.1 Precipitation, Soil Moisture, and Evapotranspiration**

Analysis of moist land-atmosphere processes properly begins with the principal hydrological forcing, the precipitation rate  $P$ . In contrast to the surface radiant fluxes,  $P$  is episodic in its forcing impact, as seen in the time series of the precipitation rate vs. the estimated moisture contained in the highly interactive top 10 cm of the underlying soil column (Figure 4) during the relatively dry 2006 (Figure 4a) versus wet 2007 (Figure 4b) warm seasons [Dong et al., 2011]. The 10-cm soil moisture values are estimated from the Soil Water Atmospheric Transfer System (SWATS) data (averaged over the closely spaced east and west soil profiles at the SGP CF) that are available from the ARM archive [Schneider et al., 2003; Bond, 2005]. Each precipitation event produces a closely following spike in soil moisture, and subsequent gradual evaporative drying of the soil, in the absence of additional precipitation.

When soil moisture exceeds a local critical value  $W_c$ , the surface evaporation  $E$  approximates the potential evaporation  $E_p$  associated with a fully wetted surface, and  $E$  is then determined mainly by the net surface radiation  $R_{net}$ , rather than by  $W$ . At the other extreme, when  $W$  falls below the vegetation wilting level  $W_{wilt}$ ,  $E$  is approximately 0. In the moisture-limited range where  $W_{wilt} < W < W_c$ ,  $E$  increases with the local soil moisture  $W$ , but also depends

in a complex way on the hydraulic properties of the soil, the biophysics of the local vegetation, and the lower atmosphere's aerodynamic resistance and humidity saturation deficit [Seneviratne et al. 2010].

Partly because of the complexity inherent in  $E$ , it is useful to define a dimensionless surface evaporative fraction  $EF$  that expresses the partitioning of the latent heat flux  $LE$  and sensible heat flux  $H$  at the surface [Betts 2004, 2009]:

$$EF = LE/(LE + H) \quad (8)$$

$EF$  tends toward a local minimum value when the Bowen ratio  $B = H/L$  is relatively large, and toward a local maximum when  $B$  is small:

$$EF = 1/(1 + B) \quad (9)$$

At the SGP CF site, the observed daily-average  $EF$  (calculated from hourly observations of  $LE$  and  $H$ ) ranges approximately between 0.2 and 0.9. Thus  $B$  seldom attains values characteristic of either very dry ( $B > 4$ ) or very wet ( $B < 0.1$ ) soils [cf. Sellers, 1969], implying that  $W$  at the CF site mostly varies over a moisture-limited range that is characteristic of a semi-arid transition zone.

To explore relationships of soil moisture with  $EF$  and other surface and low-atmosphere variables, it is also useful to define a site-specific soil moisture index [Betts 2004, 2009]:

$$SMI = (W - W_{min}) / (W_{max} - W_{min}) \quad (10)$$

Here  $W_{max}$  and  $W_{min}$  are the multi-year (1997-2008) maximum and minimum hourly values of locally observed soil moisture [cf. Schneider et al. 2003]. For this study, an index for soil

moisture at a depth of 10 cm (denoted  $SMI_{10cm}$ ) is calculated as a sensitive indicator of day-to-day soil moisture fluctuations. The corresponding  $W_{max}$  and  $W_{min}$  values are approximately 35 and  $25 \text{ kg m}^{-2}$ , respectively.

The covariation of daily-average  $EF$  with  $SMI_{10cm}$  at the SGP CF is shown in Figure 5a. The slope of the regression line is positive, confirming that moisture-limited soil conditions generally apply [e.g. Tueling et al., 2009; Dirmeyer, 2011]. The correlation coefficient and sensitivity index are found to be  $R = 0.48$  and  $I = 0.06$ , respectively. A bimodality in the distribution of  $SMI_{10cm}$  samples also is evident in Figure 5 (and is inferable from Figure 4), with more incidences of drier  $SMI_{10cm} < 0.2$  or wetter  $SMI_{10cm} > 0.8$  (some 580 or 260 samples, respectively, out of a total of about 1400 data points ) than at intermediate values.

In light of the GLACE-1 model experiments, it is pertinent to consider whether substantial amounts of precipitation at the SGP CF may result from a local recycling of soil moisture mediated by evapotranspiration. First, it should be emphasized that most of the warm-season SGP precipitation falls at night [Wallace, 1975; Riley et al., 1987; Dai et al., 1999; Zhang et al., 2008]. This nocturnal rainfall mainly derives from convective cells triggered by daytime heating of the sloping plains in the lee of the Rockies, that then propagate eastward over the SGP site [Jiang et al. 2006, Weaver and Nigam 2008, 2011]. From the large-scale studies of Ferguson and Wood [2011], Findell et al. [2011], and Taylor et al [2012], it is also reasonable to infer that little of this warm-season SGP precipitation results from locally triggered convection. Moreover, the regional studies of Lamb et al. [2012] and Ruiz-Barradas and Nigam [2013] argue for the dominance of horizontal over vertical moisture transports in precipitation formation at SGP.

At the CF site, correlations of the ARMBE observations of 1997-2008 warm-season precipitation rate  $P$  with local values of  $SMI_{10cm}$  and  $EF$  are found to be consistent with such indications that there is only a modest amount of regional moisture recycling. For instance, correlations of daytime-average  $P$  with the corresponding  $SMI_{10cm}$  and  $EF$  averages ( $R = 0.07$  and  $0.05$ , respectively) are not statistically significant. An alternative hypothesis that nighttime precipitation at SGP CF may be fueled by local evapotranspiration also is not confirmed, since the correlation ( $R = 0.16$ ) of daily (daytime + nighttime) averages of  $P$  with  $EF$  is not significant. Although the correlation of daily average  $P$  with  $SMI_{10cm}$  does yield a nominally significant value ( $R = 0.25$ ), this likely reflects a tendency for increases in  $SMI_{10cm}$  to closely align with spikes in precipitation, as shown in Figure 4. Moreover, daily average  $P$  correlates negatively ( $R = -0.13$ )--although not significantly--with the surface latent heat flux  $LE$ , probably because precipitation tends to occur in environments with high relative humidity, where the surface evaporative flux will be reduced.

#### 4.2 Other Interactions with Soil Moisture

As noted by Betts [2004, 2009], soil moisture and surface evaporation impact other surface variables such as surface relative humidity  $RH$  and surface air temperature  $T_a$  which also are included in the ARMBE database. Their covariations relative to  $SMI_{10cm}$  are depicted in Figures 5b and 5c.  $T_a$  correlates negatively with soil moisture ( $R = -0.38$ ), and  $RH$  positively ( $R = 0.51$ ). Because the surface saturation vapor pressure  $e_{sat}$  falls with decreasing  $T_a$ ,  $RH = e/e_{sat}$  will tend to rise even in the absence of a soil-moisture-driven increase in the ambient surface water vapor pressure  $e$ .

Soil moisture and covarying surface variables such as  $EF$ ,  $T_a$ , and  $RH$  also can impact the vertical levels at which clouds form in the local atmospheric boundary layer. For example,

various surface variables at SGP correlate significantly with the lifting condensation level (*LCL*), the height where buoyant air parcels become saturated, and where clouds may begin to form.

The *LCL* (in meters) can be approximated as a function of surface air temperature  $T_a$  in degrees Celsius and of the surface relative humidity percentage *RH* [Lawrence 2005]:

$$LCL = (20 + T_a/5) * (100 - RH) \quad (11)$$

The covariation of the derived *LCL* with *SMI*<sub>10cm</sub> is shown in Figure 6a. For a given surface temperature, (11) implies that an increase in relative humidity will result in a lower *LCL*. Because *RH* tends to increase with soil moisture (Figure 5b), the *LCL* also covaries inversely with *SMI*<sub>10cm</sub> (Figure 6a). While (11) ensures high correlation of the *LCL* with *RH*, the correlation of the *LCL* with *SMI*<sub>10cm</sub> ( $R = -0.52$ ,  $I = -172.16$ ) is also statistically significant.

The observed cloud base level (*CBL*) may differ, of course, from the *LCL* estimate. Measurements of the *CBL* at the SGP site obtained from the Active Remote Sensing of Cloud Layers (ARSCL) retrievals based on radar data also are accessible from the ARM archives [Clothiaux et al., 2001]. In the present study, daytime *CBL* values less than 4 km are considered, in order to select for low clouds in a growing atmospheric boundary layer that may be influenced by local soil moisture through its control of *RH*. The covariation of this observed daytime low-level *CBL* with *SMI*<sub>10cm</sub> at the CF site is shown in Figure 6b. The *CBL* also covaries inversely with *SMI*<sub>10cm</sub>, but with substantially less coherence ( $R = -0.26$ ) than the derived *LCL* ( $R = -0.52$ ); however, the sensitivity of the *CBL* to variations in soil moisture ( $I = -212.23$ ) is substantially greater than that of the *LCL* ( $I = -172.16$ ).

While soil moisture appears to influence the height of low-level clouds to some degree, it does not seem to impact the associated shortwave energetics comparably. For instance, the covariation of the daytime-average effective cloud albedo  $\alpha_c$  with  $SMI_{10cm}$  ( $R = 0.14$ ) is not statistically significant at a 99-% confidence level. Estimates of low-level cloud extent (ARMBE variable  $CLDLOW$  in Table 1) that presumably are related to  $RH$  also do not correlate significantly with  $SMI_{10cm}$  ( $R = 0.06$ ).

On the other hand,  $SMI_{10cm}$  does exert a marginally significant influence on the surface upward shortwave flux  $SW_{up}$  ( $R = -0.19$ ), which falls off as increasing soil moisture darkens the surface, thereby reducing the surface albedo  $\alpha_s$  ( $R = -0.26$ , figure not shown). The upward surface longwave flux  $LW_{up}$  correlates with  $SMI_{10cm}$  at substantially greater absolute magnitude than does  $SW_{up}$  ( $R = -0.40$  vs  $-0.19$ , figures not shown), implying that the radiative influence of soil moisture on the lower atmosphere is stronger in the longwave than the shortwave. The correlation of  $LW_{up}$  with  $SMI_{10cm}$  also is similar to that displayed by the surface air temperature  $T_a$  ( $R = -0.38$ , see Figure 5c), consistent with the observed high correlation of  $LW_{up}$  with  $T_a$  ( $R = 0.98$ , figure not shown).

### 4.3 Land-Feedback Dependencies

From Figure 5, it is seen that as  $SMI_{10cm}$  approaches zero, the surface evaporative fraction  $EF$  and relative humidity  $RH$  sharply decrease, while the surface air temperature  $T_a$  increases under such conditions of heightened moisture stress. It thus is expected that surface and lower atmospheric variables at the SGP CF site will be impacted more by local soil moisture when it is in drier states. Because of the influence of  $RH$  on the  $LCL$  and the  $CBL$ , boundary-layer cloud base levels may also be more strongly impacted under dry soil conditions.

Gross impacts of soil moisture amount on the land feedbacks can be investigated at SGP CF by distinguishing the time series of several relatively wet warm seasons (as defined by average precipitation, e.g. in the years 2002, 2004, 2007, and 2008), computing correlations  $R$  and sensitivities  $I$  of several near-surface variables with  $SMI_{10cm}$ , and comparing these with the corresponding values obtained from the time series of several relatively dry warm seasons (e.g. in the years 1998, 2003, 2005, and 2006). As an example, the wet-year versus dry-year scatter plots of the  $CBL$  are shown in Figure 7. These wet-dry comparisons (summarized in Table 3) are in accord with the expected increases in coherence and sensitivity of the covariations of surface and lower-atmospheric variables with  $SMI_{10cm}$  under drier soil conditions. The wet-dry differences in correlations  $R$  for each variable in Table 3 are statistically significant at various confidence levels that range between about 75 % for  $RH$  to about 95 % for  $EF$  [cf. <http://www.vassarstats.net/rdiff.html>].

To more systematically isolate common moisture states in gradually drying soil, composites of  $SMI_{10cm}$  also can be obtained at the same day-lag subsequent to each 1997-2008 warm-season precipitation event (whenever nonzero hourly values of  $P$  occur). As a way to quantify the associated relationships with surface and lower-atmospheric variables, the correlations of  $SMI_{10cm}$  with the corresponding values of  $EF$ ,  $RH$ ,  $T_a$ ,  $LCL$ , and  $CBL$  at the same day-lag can be computed, and then averaged over all the 1997-2008 warm-season precipitation events. The resulting composited correlations for lags up to 10 days are displayed at 2-day increments in Table 4. (Although lags up to 18 days after particular precipitation events are to be found in the ARMBE record, the sample size of the resulting composite is too small to yield meaningful statistics; hence, results are shown only up to 10 days' lag, where the typical composite sample size is about  $N = 30$ .)

From Table 4, the correlations of all variables are seen to increase after some initial drying of the soil. For example, the absolute correlations of the moisture-related variables  $EF$ ,  $RH$ ,  $LCL$ , and  $CBL$  peak at lags between 4 to 8 days, with an especially broad maximum being displayed by  $EF$ . Drying of the soil apparently enhances such hydrological land feedbacks only to a certain point, however, with gradual decoupling occurring upon further drying. From the close relationship between the  $LCL$  and  $RH$ , it is not surprising that their maximum correlations with  $SMI_{10cm}$  coincide, on average, at a 6-day lag following a precipitation event. Even though the  $CBL$  is less tightly coupled with  $RH$ , it also shows a maximum correlation at a 6-day lag. In contrast to the moisture-related variables, however, the correlation of surface air temperature  $T_a$  with  $SMI_{10cm}$ , becomes increasingly negative as the soil continues to dry out after precipitation events, reaching a value  $R = -0.33$  at 10-days lag.

Another approach for identifying instances of relatively strong land feedback is to isolate daytime cases when boundary-layer cumulus clouds grow from surface convection, since then the opportunity to discern the impact of the surface on low-level clouds may be better. For example, both forced (“thin”) and active (“thick”) shallow cumulus (SHCU) clouds form at the SGP site when moist thermal updrafts driven by local surface sensible heating are present [Zhang and Klein, 2013]. By convolving indices of the observed occurrences of thin or thick SHCU clouds [personal communication, Y. Zhang], with the entire 1997-2008 warm-season record of hourly  $CBL$  data at SGP, daytime-average values of the  $CBL$  for both types of SHCU clouds can be computed.

Scatter plots of the covariation of the daytime averages of thin-or thick-SHCU  $CBL$  with  $RH$  and  $SMI_{10cm}$  are shown in Figure 8. At the SGP CF site, incidences of SHCU clouds are sporadic,

with a total of only about 70 occurrences during the 1997-2008 warm seasons; of these, 43 are spaced at least 5 days apart, and so can be treated as statistically independent events. A correlation  $R$  then must be greater than about 0.42 in absolute value to be regarded as statistically significant at a 99 % confidence level. The correlation of SHCU  $CBL$  with  $RH$  ( $R = -0.54$ ) easily passes this threshold, while the correlation with  $SMI_{10cm}$  ( $R = -0.31$ ) does not.

Like the all-cloud  $CBL$  of Figure 6b, the SHCU  $CBL$  varies inversely with both  $RH$  and  $SMI_{10cm}$ ; but the daytime-average covariations of the SHCU  $CBL$  with  $RH$  ( $R = -0.54$ —Figure 8a) and with  $SMI_{10cm}$  ( $R = -0.31$ —Figure 8b) are more coherent than the corresponding correlations of the all-cloud  $CBL$  with  $RH$  and  $SMI_{10cm}$  ( $R = -0.33$ —figure not shown, and  $-0.26$ —Figure 6b, respectively). This result confirms the supposition that the influence of the surface on low-level clouds is stronger when they are known to originate from surface-based convection. (It should also be noted that the daytime-average correlation of the SHCU  $CBL$  with  $RH$  is considerably less than what is obtained from *hourly* samples--see Figure 14 of Zhang and Klein [2013].)

## 5. Discussion

In this study, the ARMBE and supplemental field observations make possible a fairly comprehensive investigation of local warm-season land-atmosphere interactions at the SGP CF site. The energetic forcing of the atmosphere on the surface is seen to be substantial, and to largely determine the land's response, in the form of turbulent heat fluxes. In contrast, the land's energetic feedbacks on the atmosphere are comparatively weak. For example, the impact of 10-cm soil moisture on surface and cloud shortwave radiant fluxes appears to be only marginally

significant. However, because of its influence on surface temperature, soil moisture does seem to have a greater impact on the upward longwave flux.

At the SGP CF site, the hydrological forcing of the land by precipitation also predominates over the land's moist feedbacks, with little evidence that the SGP CF soil moisture triggers much precipitation via local moisture recycling. This outcome is consistent with the known remote origins of most of the precipitation that falls at SGP, as well as the implications of several other observationally based studies (e.g. Ferguson and Wood [2011], Lamb et al. [2012], Taylor et al. [2012], Ruiz-Barradas and Nigam [2013]). Much of the time also, the surface evaporative fraction  $EF$  exhibits a fairly weak dependence on the 10-cm soil moisture index  $SMI_{10cm}$ . However, as the soil begins to dry out after a precipitation event,  $EF$  couples more tightly with soil moisture. Similar effects are also observed in surface relative humidity and temperature, as well as in the heights of boundary-layer cloud bases. On days when shallow cumulus clouds are initiated, presumably by thermal updrafts associated with surface sensible heating, the coupling with soil moisture also grows stronger.

The observationally based perspectives cited above would appear to call into question the GLACE-1 model ensemble mean result, which implied that an especially strong coupling of local soil moisture and precipitation prevails over the central U.S. under present-day summer conditions. The GLACE-1 models therefore may have substantially overestimated the strength of this coupling. Nevertheless, because the central U.S. is situated in a moisture-stressed transition zone with potential for strong land-atmosphere coupling (e.g. Ferguson et al. [2012]), it may still be a “hot spot” relative to many other parts of the world.

Moreover, if the local climatic regime were to shift to generally drier conditions (e.g. as a result of future greenhouse-induced warming), the present study implies that these land feedbacks would become stronger, possibly also inducing more frequent or intense heat waves (Seneviratne et al. [2006], Fischer et al. [2007], Jaeger and Seneviratne [2011], Lorenz et al. [2010, 2012], Miralles et al. [2012], Orth and Seneviratne [2012]). Such a prospect also seems consistent with land-atmosphere interactions in the idealized model of Lintner et al. [2013], and in the global-warming simulations analyzed by Dirmeyer et al. [2012, 2013].

## **6. Future Investigations**

The seeming divergence between the inferences drawn from observations versus simulations begs the question ‘how might today’s global climate models be made more realistic in their representation of land-atmosphere coupling mechanisms, such as are pertinent to the U.S. Great Plains?’

For seasonal climate prediction, part of the answer may entail using precipitation observations to initialize model soil moisture. For example, in the GLACE Phase 2 (GLACE-2) numerical experiments where this protocol was adopted, the model ensemble-mean maximum in precipitation forecast skill was located in the U.S. Northern Great Plains and Mountain West, rather than in the central U.S. [Koster et al., 2011]. This result also appears to be in better agreement with the Findell et al. [2011] observationally based estimates of linkages between surface evaporation and afternoon convective precipitation.

On the other hand, Klein et al. [2006] showed that even when soil moisture was realistically initialized in a participating GLACE model, its simulation inadequately captured the nocturnal

precipitation associated with eastward propagating convective cells in the lee of the Rockies, resulting in a large warm/dry model bias over the SGP region. This is a general failing of coarse-resolution global models [e.g. Lee et al. ,2007].

A parameterization-focused evaluation of today's global climate model simulations of cloud-convective processes and their relationship to land-atmosphere coupling over the central U.S. would thus seem to be a high priority. It is therefore fortuitous that climate model behaviors now can be evaluated in a more detailed fashion than was generally possible in the GLACE-1 era. For instance, it is currently feasible to initialize a global atmospheric climate model realistically from reanalyses, to run it in weather-prediction mode, and to compare its forecasts with local, high-frequency observations as a means of evaluating convective or other atmospheric model parameterizations (e.g. see the SGP-centric studies by Phillips et al. [2004], Xie et al. [2004], Williamson et al. [2005], as well as the multi-model experiment described by Williams et al. [2013]). If such a model's soil moisture also were initialized from observed precipitation, as in the GLACE-2 experiment, forecast deviations from the observed SGP land-atmosphere covariances (such as are described in the present study), could potentially highlight flaws in the model's land-surface or boundary-layer parameterizations. This diagnosis, in turn, would motivate and guide improvements in the associated model representations [e.g. Lorenz et al., 2012]. (For observed land-atmosphere covariance relationships to provide meaningful evaluation criteria for the typical global climate model at 50-200 kilometer grid scale, soil moisture and available surface and boundary-layer variables from SGP sites surrounding the CF probably would need to be utilized as well.)

It should also be noted that nocturnal, convective cells propagating eastward from the Rockies recently have been more successfully simulated by high-resolution mesoscale models that include complex cloud-convection representations [Tao et al., 2013] or by GCMs with embedded cloud-resolving models [Pritchard et al.[2011]). In their observational study of continental convection, Taylor et al. [2012] also posited an important role for mesoscale circulations in triggering continental convection over drier soils. Improved simulation of warm-season land-atmosphere interactions thus may depend on properly representing the mesoscale effects of convection and its dependence on surface processes.

In this respect, the mesoscale testbed implemented by Santanello et al. [2009, 2011a,b] offers a promising diagnostic protocol. They have conducted process studies of SGP land-atmosphere interactions by employing a regional atmospheric mesoscale model that is coupled to a suite of different boundary layer and land surface schemes, and that is evaluated locally against ARM observations (e.g. at the CF and at another SGP site in southwest Kansas site). By employing thermodynamic mixing diagrams [Betts, 1992] to express the covariation of observed atmospheric potential temperature and moisture in the vertical column situated over a 1x1-kilometer model grid box, Santanello et al. have identified multiple pathways by which the local land and atmosphere interact on a diurnal time scale. They also have developed metrics to quantify the local land-atmosphere coupling strength associated with each model configuration, and to evaluate these against the corresponding observationally based metrics.

Thus, even though land-atmosphere coupling appears to entail more complex interactions than were initially recognized, there are new tools at hand to diagnose and evaluate the details of these interactions. It is likely, nonetheless, that an accurate identification and effective correction

of the sources of model errors in representing different facets of land-atmosphere coupling will continue to prove challenging.

## Notation

$\alpha_c$	Effective short-wave cloud albedo, dimensionless
$\alpha_s$	Land surface albedo, dimensionless
$\gamma$	Slope of least-squares regression line, variable units
$\sigma$	Multi-year standard deviation
$B$	Bowen ratio, dimensionless
$CBL$	Cloud base level, m
$CLDLow$	Low-level cloud cover, %
$E$	Surface evapotranspiration, mm hr <sup>-1</sup>
$E_p$	Potential evaporation, mm hr <sup>-1</sup>
$EF$	Evaporative Fraction, dimensionless
$e$	Water vapor pressure, Pa
$e_{sat}$	Water vapor saturation pressure, Pa
$G$	Ground heat flux, W m <sup>-2</sup>
$H$	Surface sensible heat flux, W m <sup>-2</sup>
$I$	Sensitivity index, various units
$LE$	Surface latent heat flux, W m <sup>-2</sup>
$LCL$	Lifting Condensation Level, m
$LW_{dn}$	Surface downward long-wave flux, W m <sup>-2</sup>
$LW_{up}$	Surface downward long-wave flux, W m <sup>-2</sup>
$LW_{net}$	Surface net long-wave flux, W m <sup>-2</sup>
$M$	Number of non-missing hourly samples per day
$N$	Estimated number of statistically independent samples
$P$	Precipitation rate, mm hr <sup>-1</sup>
$P_{day}$	Daytime precipitation rate, mm hr <sup>-1</sup>
$R$	Temporal correlation coefficient, dimensionless
$R_{net}$	Surface net total radiation, W m <sup>-2</sup>
$RH$	Surface relative humidity, %
$SMI$	Soil Moisture Index, dimensionless
$SMI_{10cm}$	$SMI$ calculated from moisture in the top 10 cm of soil
$SW_{dn}$	Surface downward short-wave flux, W m <sup>-2</sup>
$SW_{dn\ clr}$	Surface clear-sky downward short-wave flux, W m <sup>-2</sup>
$SW_{dn\ TOA}$	Downward short-wave flux at top of atmosphere, W m <sup>-2</sup>
$SW_{up}$	Surface upward short-wave flux, W m <sup>-2</sup>
$SW_{net}$	Surface net short-wave flux, W m <sup>-2</sup>
$T_a$	Surface air temperature, K
$T_s$	Surface skin temperature, K
$W$	Soil moisture, kg m <sup>-2</sup>
$W_c$	Local critical value of soil moisture, kg m <sup>-2</sup>
$W_{wilt}$	Local value of soil moisture unreachable by vegetation roots, kg m <sup>-2</sup>
$W_{max}$	Maximum multi-year value of soil moisture, kg m <sup>-2</sup>
$W_{min}$	Minimum multi-year value of soil moisture, kg m <sup>-2</sup>
$x$	Arbitrary “independent” variable, diverse units
$y$	Arbitrary “dependent” variable, diverse units

## **Acknowledgements**

We gratefully acknowledge the USDOE ARM Program for supplying the ARMBE data sets, and our colleagues Yunyan Zhang and Shaocheng Xie for sharing additional ARM datasets and for offering comments that improved this paper. We also greatly appreciate Charles Doutriaux's expert assistance with numerous data-processing problems. This work was funded by the U.S. Department of Energy (USDOE) Office of Science under its Atmospheric System Research (ASR) Program, and was performed at the Lawrence Livermore National Laboratory under Contract DE-AC52-07NA27344.

## References

- Ackerman, T.P., and G.M. Stokes (2003), The Atmospheric Radiation Measurement Program. *Physics Today*, 56, 38-44.
- Betts, A.K. (1992), FIFE atmospheric boundary layer budget methods, *J. Geophys. Res.*, 97, 18523-18531.
- Betts, A.K. (2004), Understanding hydrometeorology using global models, *Bull. Am. Meteorol. Soc.*, 85, 1673-1688, doi:10.1175/BAMS-85-11-1673.
- Betts, A.K. (2009), Understanding land-surface-atmosphere coupling in observations and models, *J. Adv. Modeling Earth Systems*, 1, doi:10.3894/JAMES.2009.1.4, 18 pp.
- Betts, A.K., J.H. Ball, A.C.M. Beljaars, M.J. Miller, and P. Viterbo (1996), The land-surface-atmosphere interaction: A review based on observational and global modeling perspectives, *J. Geophys. Res.*, 101, 7209-7225.
- Bond, D., (2005), Soil water and temperature system (SWATS) handbook, ARM Technical Report TR-063, U.S. Department of Energy, Washington, D.C.
- Bulmer, M.G. (1979), *Principles of Statistics*, ISBN 0-486-63760-3, Dover Publications Inc., New York, NY, 252 pp.
- Clothiaux, E.E, and Coauthors (2001), The ARM Millimeter Wave Cloud Radars (MMCRs) and the Active Remote Sensing of Clouds (ARSCL) Value Added Product (VAP), DOE Tech. Memo. ARM VAP-002.1, U.S. Department of Energy, Washington, D.C.
- Cook, D.R., (2011), Energy balance Bowen ratio handbook. ARM Technical Report TR-037, USDOE Office of Science, Washington, D.C.
- Dai, A., F. Giorgi, and K.E. Trenberth (1999), Observed and model-simulated diurnal cycles of precipitation over the contiguous United States, *J. Geophys. Res.*, 104, 6377-6402.
- Dirmeyer, P.A. (2011), The terrestrial segment of soil moisture-climate coupling. *Geophys. Res. Lett.*, 38, L16702, doi:10.1029/2011GL048268.
- Dirmeyer, P.A., R.D. Koster, and Z. Guo (2006), Do global models properly represent the feedback between land and atmosphere? *J. Hydrometeor.*, 7, 1177-1198.
- Dirmeyer, P.A., B.A. Cash, J.L. Kinter III, C. Stan, T. Jung, L. Marx, P. Towers, N. Wedi, J.M. Adams, E.L. Altshuler, B. Huang, E.K. Jin, and J. Manganello (2012), Evidence for enhanced land-atmosphere feedback in a warming climate, *J. Hydrometeor.*, 13, 981-995.
- Dirmeyer, P.A., Y. Jin, B. Singh, and X. Yan (2013), Evolving land-atmosphere interactions over North America from CMIP5 simulations, *J. Climate*, 26, 7313-7326.
- Dong, X., B. Xi, A. Kennedy, Z. Feng, J.K. Entin, P.R. Houser, R.A. Schiffer, T. L'Ecuyer, W.S. Olson, K-L. Hsu, W.T. Liu, B. Lin, Y. Deng, and T. Jiang (2011), Investigation of the 2006 drought and 2007 flood extremes at the Southern Great Plains through an integrative analysis of observations, *J. Geophys. Res.*, 116, D03204, doi:10.1029/2010JD014776.
- Ferguson, C.R., and E.F. Wood (2011), Observed land-atmosphere coupling from satellite remote sensing and reanalysis, *J. Hydrometeor.*, 12, 1221-1254.

- Ferguson, C. R., E. F. Wood, and R. K. Vinukollu (2012), A Global intercomparison of modeled and observed land-atmosphere coupling, *J Hydrometeor.*, *13*, 749-784.
- Findell, K.L., P. Gentine, B.R. Lintner, and C. Kerr (2011), Probability of afternoon precipitation in eastern United States and Mexico enhanced by high evaporation, *Nature Geosci.*, *4*(7), 434-439, doi:10.1038/ngeo1174.
- Fischer, E.M., S.I. Seneviratne, D. Luthi, and C. Schar (2007), Contribution of land-atmosphere coupling to recent European summer heat waves, *Geophys. Res. Lett.*, *34*, L06707, doi:10.1029/2006GL029068.
- Guo, Z., and Coauthors (2006), GLACE: The Global Land-Atmosphere Coupling Experiment. Part II: Analysis, *J. Hydrometeor.*, *7*, 611-625.
- Jaeger, E.B., and S.I. Seneviratne (2011), Impact of soil moisture-atmosphere coupling on European climate extremes and trends in a regional model, *Climate Dyn.*, *36*, 1919-1939, doi: 10.1007/s00382-010-0780-8.
- Jiang, X., N.-C. Lau, and S.A. Klein (2006), Role of eastward propagating convection systems in the diurnal cycle and seasonal mean of summertime rainfall over the U.S. Great Plains, *Geophys. Res. Lett.*, *33*, L19809, doi:10.1029/2006GL027022.
- Klein, S., X. Jiang, J. Boyle, S. Malyshev, and S. Xie (2006), Diagnosis of the summertime warm and dry bias over the U.S. Southern Great Plains in the GFDL climate model using a weather forecasting approach, *Geophys. Res. Lett.*, *33*, L18805, doi:10.1029/2006GL027567.
- Koster, R.D., and Coauthors (2004), Regions of strong coupling between soil moisture and precipitation, *Science*, *305*, 1138-1140.
- Koster, R.D., and Coauthors (2006), GLACE: The Global Land-Atmosphere Coupling Experiment. Part I: Overview, *J. Hydrometeor.*, *7*, 590-610.
- Koster, R.D., and Coauthors (2011), The second phase of the global land-atmosphere coupling experiment: Soil moisture contributions to subseasonal forecast skill, *J. Hydrometeor.*, *12*, 805-822.
- Lamb, P.J., D.H. Portis, and A. Zangvil (2012): Investigation of large-scale atmospheric moisture budget and land surface interactions over U.S. Southern Great Plains including for CLASIC (June 2007), *J. Hydrometeor.*, *13*, 1719-1738.
- Lawrence, M.G. (2005), The relationship between relative humidity and the dew point temperature in moist air: A simple conversion and applications, *Bull. Am. Meteor. Soc.*, *86*, 225-233.
- Lee, M.I., S.D. Schubert, M.J. Suarez, I.M. Held, N.C. Lau, J.J. Ploshay, A. Kumar, H.K. Kim, and J.K.E. Schemm (2007), An analysis of the warm-season diurnal cycle over the continental United States and northern Mexico in general circulation models, *J. Hydrometeor.*, *8*, 344-366.
- Lintner, B.R., P. Gentine, K.L. Findell, F. D'Andrea, A.H. Sobel, and G.D. Salvucci (2013), An idealized prototype for large-scale land-atmosphere coupling, *J. Climate*, *26*, 2379-2389.
- Long, C.N., and Y. Shi (2006), The QCRad value added product: Surface radiation measurement quality control testing, including climatologically configurable limits, *Atmospheric*

- Radiation Measurement Program Tech. Rep. ARM TR-074, 69 pp. [Available online at [www.arm.gov/publications/tech\\_reports/arm-tr-074.pdf](http://www.arm.gov/publications/tech_reports/arm-tr-074.pdf).]
- Long, C.N., and Y. Shi (2008), An automated quality assessment and control algorithm for surface radiation measurements, *The Open Atmos. Sci. Journal*, 2, 23-37, doi: 10.2174/1874282300802010023..
- Lorenz, R., E.B. Jaeger, and S.I. Seneviratne (2010), Persistence of heat waves and its link to soil moisture memory, *Geophys. Res. Lett.*, 37, L09703, doi: 10.1029/2010GL042764.
- Lorenz, R., E.L. Davin, and S.I. Seneviratne (2012), Modeling land-climate coupling in Europe: Impact of land surface representation on climate variability and extremes, *J. Geophys. Res.*, 117, doi:10.1029/2012D017755.
- Mather, J.H., and J.W. Voyles (2013), The ARM Climate Research Facility: A review of structure and capabilities. *Bull. Amer. Meteor. Soc.*, 94, 377-392.
- Miralles, D.G., M.J. van den Berg, A.J. Teuling, and R.A.M. de Jeu (2012), Soil moisture-temperature coupling: A multiscale observational analysis, *Geophys. Res. Letters*, 39, L21707.
- Morris, V.I. (2005), Total sky imager handbook, ARM Technical Report TR-017, USDOE Office of Science, Washington, D.C.
- Orth, R., and S.I. Seneviratne (2012), Analysis of soil moisture memory from observations in Europe, *J. Geophys. Res.*, 117, D15115.
- Orlowsky, B., and S.I. Seneviratne (2010), Statistical analyses of land-atmosphere feedbacks and their possible pitfalls, *J. Climate*, 23, 3918-3932.
- Phillips, T.J., G. L. Potter, D. L. Williamson, R. T. Cederwall, J.S. Boyle, M. Fiorino, J. J. Hnilo, Jerry G. Olson, S. Xie, and J. J. Yio (2004), Evaluating parameterizations in general circulation models: Climate simulation meets weather prediction, *Bull. Amer. Meteor. Soc.*, 85, 1903-1915.
- Pritchard, M.S., M.W. Moncrieff, and R.C.J. Somerville (2011), Orographic propagating precipitation systems over the United States in a global climate model with embedded explicit convection, *J. Atmos. Sci.*, 68, 1821-1840.
- Riley, G.T., M.G. Landin, and L.F. Bosart (1987), The diurnal variability of precipitation across the central Rockies and adjacent Great Plains, *Mon. Weather Rev.*, 115, 1161-1172.
- Ritsche, M.T. (2008), Surface meteorological observation system handbook, ARM Technical Report TR-031, USDOE Office of Science, Washington, D.C.
- Ruiz-Barradas, A., and S. Nigam (2006), Great Plains hydroclimatic variability: The view from the North American Regional Reanalysis, *J. Climate*, 19, 3004-3010.
- Ruiz-Barradas, A., and S. Nigam (2013), Atmosphere-land surface interactions over the Southern Great Plains: Characterization from Pentad Analysis of DOE ARM field observations and NARR, *J. Climate*, 26, 875-886.
- Santanello, J.A., C.D. Peters-Lidard, S.V. Kumar, C. Alonge, and W.-K. Tao (2009), A modeling and observational framework for diagnosing local land-atmosphere coupling on diurnal time scales, *J. Hydrometeor.*, 10, 577-599.

- Santanello, J.A., C. Ferguson, M. Ek, P. Dirmeyer, O. Tuinenburg, C. Jacobs, C. van Heerwaarden, K. Findell, P. Gentile, and B. Lintner (2011), Local land-atmosphere coupling (LoCo) research: Status and results. *GEWEX News*, Vol. 21, No. 4, 7-9.
- Santanello, J.A., C. D. Peters-Lidard, and S.V. Kumar (2011), Diagnosing the sensitivity of local land-atmosphere coupling via the soil moisture-boundary layer interaction, *J. Hydrometeor.*, 12, 766-786.
- Schneider, J.M., D.K. Fisher, R.L. Elliott, G.O. Brown, and C.P. Bahrmann (2003), Spatiotemporal variation in soil water: First results from the ARM SGP CART Network, *J. Hydrometeor.*, 4, 106-120.
- Sellers, W.D. (1969), *Physical Climatology*, University of Chicago Press, Chicago.
- Seneviratne, S.I., D. Luthi, M. Litschi, and C. Schar (2006), Land-atmosphere coupling and climate change in Europe, *Nature*, 443, 205-209.
- Seneviratne, S.I., T. Corti, E.L. Davin, M. Hirschi, E.B. Jaeger, I. Lehner, B. Orlowsky, and A.J. Teuling (2010), Investigating soil moisture-climate interactions in a changing climate: A review, *Earth Sci. Rev.*, 99, 125-161.
- Tao, W-K., D. Wu, T. Matsui, C. Peters-Lidard, S. Lang, A. Hou, M. Rienecker, W. Petersen, and M. Jensen (2013), Precipitation intensity and variation during MC3E: A numerical modeling study, *J. Geophys. Res.*, 118, 1-20.
- Taylor, C.M., R.A.M. de Jeu, F. Guichard, P.P. Harris, and W.A. Dorigo (2012), Afternoon rain more likely over drier soils, *Nature*, 489, 423-426.
- Teuling, A.J., M. Hirschi, A. Ohmura, M. Wild, M. Reichstein, P. Ciais, N. Buchmann, C. Ammann, L. Montagnani, A.D. Richardson, G. Wohlfahrt, and S. I. Seneviratne (2009), A regional perspective on trends in continental evaporation, *Geophys. Res. Lett.*, 36, L02404, doi:10.1029/2008GL036584.
- Wallace, J.M. (1975), Diurnal variations of precipitation and thunderstorm frequency over the conterminous United States, *Mon. Weather Rev.* 103, 406-419.
- Weaver, S.J., and S. Nigam (2008), Variability of the Great Plains low-level jet: Large-scale circulation context and hydroclimate impacts, *J. Climate*, 21, 1532-1551.
- Weaver, S.J., and S. Nigam (2011), Recurrent supersynoptic evolution of the Great Plains low-level jet, *J. Climate*, 24, 575-582.
- Williams, K.D., A. Bodas-Salcedo, M. Deque, S. Fermepin, B. Medeiros, M. Watanabe, C. Jakob, S.A. Klein, C.A. Senior, and D.L. Williamson (2013), The Transpose-AMIP II experiment and its application to the understanding of Southern Ocean cloud biases in climate models, *J. Climate*, 26, 3258-3274.
- Williamson, D., J. Boyle, R. Cederwall, M. Fiorino, J. Hnilo, J. Olson, T. Phillips, G. Potter, and S.C. Xie (2005), Moisture and temperature balances at the Atmospheric Radiation Measurement Southern Great Plains Site in forecasts with the Community Atmospheric Model (CAM2), *J. Geophys. Res.*, 110, D15516, doi:10.1029/2004JD005109.
- Xie, S.C., M. Zhang, J.S. Boyle, R.T. Cederwall, G.L. Potter, and W. Lin (2004), Impact of a revised convective triggering mechanism on Community Atmosphere Model, Version 2

simulations: Results from short-range weather forecasts, *J. Geophys. Res.*, *109*, D14102, doi:10.1029/2004JD004692.

Xie, S.C., and Coauthors (2010), ARM Climate Modeling Best Estimate Data: A new product for climate studies, *Bull. Amer. Meteor. Soc.*, *91*, 13-20. (See also the URL [http://science.arm.gov/wg/cpm/scm/best\\_estimate.html](http://science.arm.gov/wg/cpm/scm/best_estimate.html) for data set details.)

Zhang, Y., and Coauthors (2008), On the diurnal cycle of deep convection, high-level cloud, and upper troposphere water vapor in the Multiscale Modeling Framework, *J. Geophys. Res.*, D16105, doi:10.1029/2008JD009905.

Zhang, Y., and S.A. Klein (2010), Mechanisms affecting the transition from shallow to deep convection over land: Inferences from observations of the diurnal cycle collected at the ARM Southern Great Plains Site. *J. Atmos. Sci.*, *67*, 2943-2959.

Zhang, Y., and S. A. Klein (2013), Factors controlling the vertical extent of fair-weather shallow cumulus over land: Investigation of diurnal-cycle observations collected at the ARM Southern Great Plains site, *J. Atmos. Sci.*, *70*, 1297-1315.

## Tables

Table 1: Selected ARM Best Estimate (ARMBE—cf. Xie et al. [2010]) and other ARM-observed variables considered in this study (the latter denoted by shading), as well as their respective symbolic notations, measuring instruments, estimated measurement root mean square error (RMSE) in the units of the observed variable, and pertinent references. All variables are observed at hourly frequencies during the 1997-2008 May-August warm seasons at the Central Facility (CF) of the Atmospheric Radiation Measurement (ARM) U.S. Southern Great Plains Site near Lamont, Oklahoma. See also <http://www.arm.gov/data/vaps/armbe> for further instrumental details pertaining to the ARMBE data sets.

Variable	Symbol	Instruments	RMSE	Reference
Cloud base level	<i>CBL</i>	Millimeter radar, lidar	50 m	Clothiaux et al. [2001]
Low-level cloud cover	<i>CLDLow</i>	Millimeter radar, total sky imager	10 %	Clothiaux et al. [2001], Morris [2005]
Surface sensible heat flux	<i>H</i>	Energy Balance Bowen Ratio (EBBR): net radiometer; anemometer & wind vane; temperature, relative humidity, soil moisture and heat flux probes	30 W m <sup>-2</sup>	Cook [2011]
Surface latent heat flux	<i>LE</i>		20 W m <sup>-2</sup>	
Surface downward longwave flux	<i>LW<sub>dn</sub></i>	Pyrgeometer	10 W m <sup>-2</sup>	Long and Shi [2006, 2008]
Surface upward long-wave flux	<i>LW<sub>up</sub></i>	Pyrgeometer	5 W m <sup>-2</sup>	Long and Shi [2006, 2008]
Precipitation rate	<i>P</i>	Tipping bucket rain gauge	0.02 mm hr <sup>-1</sup>	Ritsche [2008]
Surface relative humidity	<i>RH</i>	Temperature/relative humidity thermistor	1 %	Ritsche [2008]
Surface clear-sky downward shortwave flux	<i>SW<sub>dn clr</sub></i>	Pyranometer-derived	20 W m <sup>-2</sup>	Long and Shi [2006, 2008]
Surface downward shortwave flux	<i>SW<sub>dn</sub></i>	Pyranometer	20 W m <sup>-2</sup>	Long and Shi [2006, 2008]
Surface upward shortwave flux	<i>SW<sub>up</sub></i>	Pyranometer	5 W m <sup>-2</sup>	Long and Shi [2006, 2008]
Surface air temperature	<i>T<sub>a</sub></i>	Temperature/relative humidity thermistor	0.4 K	Ritsche [2008]
Soil moisture	<i>W</i>	Heat-dissipation matric potential sensor	2.5 kg m <sup>-2</sup>	Schneider et al.[2003], Bond[2005]

Table 2: Summary of correlations  $R$  and sensitivities  $I$  for surface radiant and turbulent fluxes, all with respect to the effective shortwave cloud albedo  $\alpha_c$ .

Variable	Correlation $R$	Sensitivity $I$
$SW_{net}$	-0.65	- 54.17
$LW_{net}$	0.71	14.88
$R_{net}$	-0.55	-37.76
$LE$	-0.38	-22.13
$H$	-0.29	-10.35

Table 3: Listing of correlation coefficients  $R$  and sensitivity indices  $I$  of variables covarying with respect to 10-cm soil moisture index  $SMI_{10cm}$ . The values of  $SMI_{10cm}$  and of the covarying variables are drawn from the warm seasons of four relatively wet years (2002, 2004, 2007, and 2008), or of four relatively dry years (1998, 2003, 2005, and 2006). See the text for further details.

Variable	$R, I$ in wet years	$R, I$ in dry years
$EF$	0.33, 0.04	0.57, 0.07
$RH$	0.42, 4.55	0.51, 6.48
$T_a$	-0.27, -1.12	-0.43, -2.05
$LCL$	-0.43, -120.74	-0.52, -178.31
$CBL$	-0.14, -104.60	-0.27, -222.05

**Table 4:** Composite-average correlations  $R$  of surface or lower atmospheric variables vs 10-cm soil moisture index  $SMI_{10cm}$ , as a function of the number of days lagging (“ld”) precipitation events during the 1997-2008 warm seasons at the SGP Central Facility site. Each variable’s maximum correlation with  $SMI_{10cm}$  over the range of lagdays 2-10 also is denoted by boldface font.

Variable	$R$ (ld2)	$R$ (ld4)	$R$ (ld6)	$R$ (ld8)	$R$ (ld10)
$EF$	0.45	<b>0.57</b>	0.47	0.55	0.30
$RH$	0.42	0.43	<b>0.53</b>	0.29	0.24
$T_s$	-0.20	-0.26	-0.27	-0.25	<b>-0.33</b>
$LCL$	-0.44	-0.45	<b>-0.52</b>	-0.29	-0.25
$CBL$	-0.12	-0.23	<b>-0.35</b>	-0.11	-0.05

## Figure Captions

Figure 1: Scatter plots of daily averages of  $SW_{net}$  (in  $\text{W m}^{-2}$ ) versus effective cloud albedo  $\alpha_c$  are shown in (a), and of the surface total net radiation  $R_{net}$  (in  $\text{W m}^{-2}$ ) versus  $\alpha_c$  in (b) for the 1997-2008 May-August warm seasons at the SGP site. The least-squares regression line, as well as the correlation coefficient  $R$  and sensitivity index  $I$  also are shown in each plot (see text for details).

Figure 2: As in Figure 1, except for the surface net long-wave radiation  $LW_{net}$  (in  $\text{W m}^{-2}$ ) versus effective cloud albedo  $\alpha_c$  in (a), and  $LW_{net}$  versus surface relative humidity  $RH$  (in %) in (b).

Figure 3: As in Figure 1, except for the surface latent heat flux  $LE$  (in  $\text{W m}^{-2}$ ) versus effective cloud albedo  $\alpha_c$  in (a) and the surface sensible heat flux  $H$  versus the difference  $LE - R_{net}$  of the surface latent heat flux and the net radiation (all in  $\text{W m}^{-2}$ ) in (b).

Figure 4: Warm-season hourly time series of SGP precipitation rate  $P$  ( $\text{mm hr}^{-1}$  in blue) versus soil moisture offset  $\Delta W = (W_{10cm} - 25) \text{ kg m}^{-2}$  for the top 10 cm of soil (in green) are shown for the anomalously dry year 2006 in (a), and for the anomalously wet year 2007 in (b).

Figure 5: As in Figure 1, except for the surface evaporative fraction  $EF$  in (a), the surface relative humidity  $RH$  in (b), and the surface air temperature  $T_a$  in (c), all with respect to the 10-cm soil moisture index  $SMI_{10cm}$ .

Figure 6: As in Figure 1, except for the derived lifting condensation level  $LCL$  (in meters) in (a), and the observed daytime-average cloud base level  $CBL$  for those clouds with bases below 4 km in (b), both with respect to the 10-cm soil moisture index  $SMI_{10cm}$ .

Figure 7: As in Figure 1, except for the observed cloud base level  $CBL$  for those clouds with bases below 4 km versus the 10-cm soil moisture index  $SMI_{10cm}$  for (a) the wet warm seasons of 2002, 2004, 2007, and 2008, and (b) for the dry warm seasons of 1998, 2003, 2005, and 2006.

Figure 8: As in Figure 1, except for the observed daytime-average cloud base level  $CBL$  during occurrences of forced (“thin”) or active (“thick”) shallow cumulus clouds versus surface relative humidity  $RH$  in (a), and versus the 10-cm soil moisture index  $SMI_{10cm}$  in (b). See the text for further details.

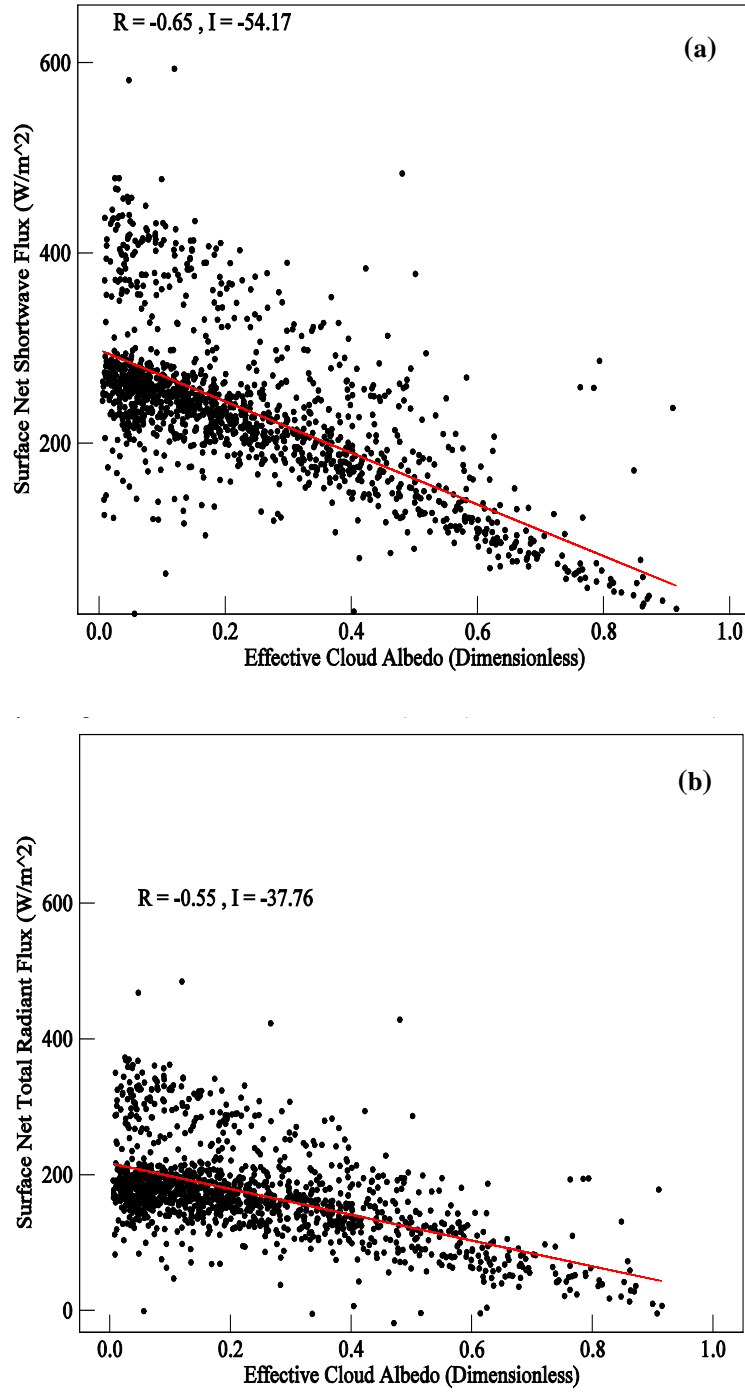


Figure 1: Scatter plots of daily averages of  $SW_{net}$  (in  $\text{W m}^{-2}$ ) versus effective cloud albedo  $\alpha_c$  are shown in (a), and of the surface total net radiation  $R_{net}$  (in  $\text{W m}^{-2}$ ) versus  $\alpha_c$  in (b) for the 1997-2008 May-August warm seasons at the SGP site. The least-squares regression line, as well as the correlation coefficient  $R$  and sensitivity index  $I$  also are shown in each plot (see text for details).

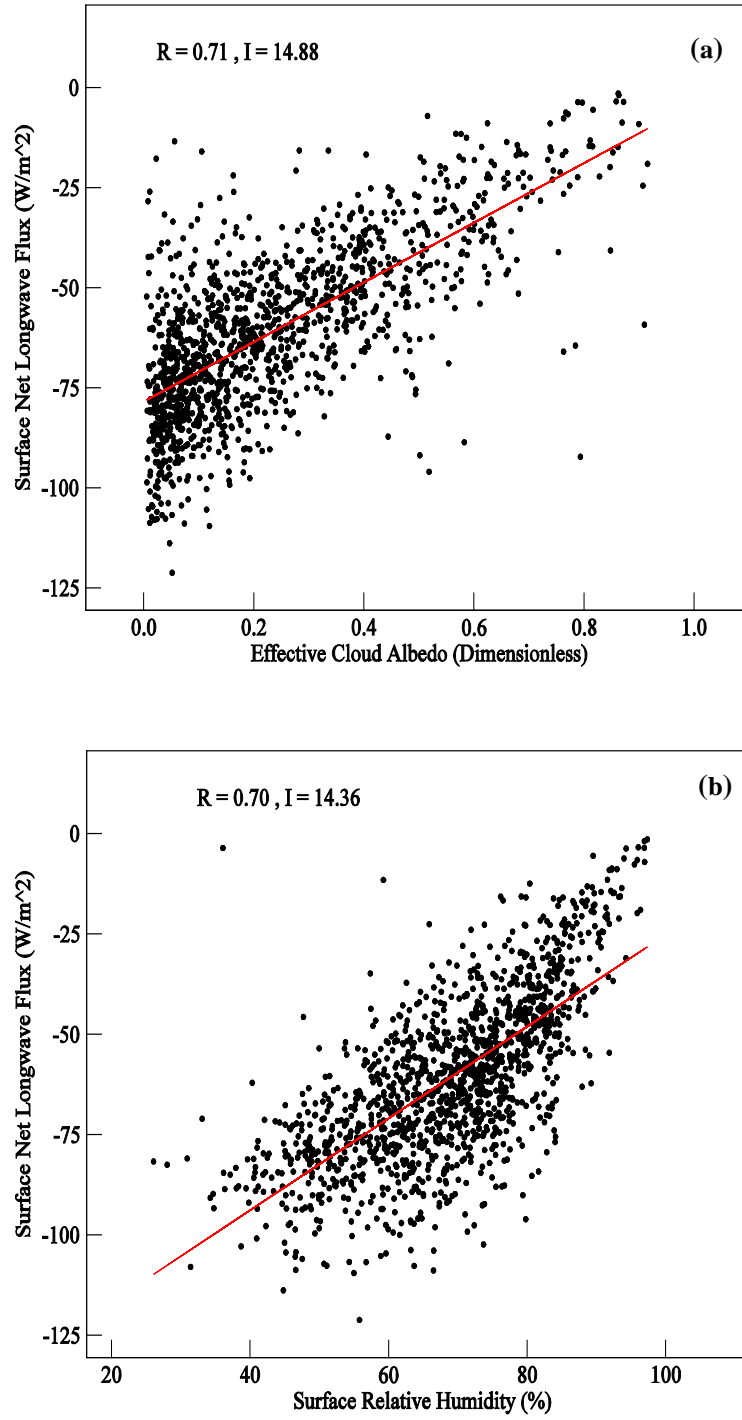


Figure 2: As in Figure 1, except for the surface net long-wave radiation  $LW_{net}$  (in  $\text{W m}^{-2}$ ) versus effective cloud albedo  $\alpha_c$  in (a), and  $LW_{net}$  versus surface relative humidity  $RH$  (in %) in (b).

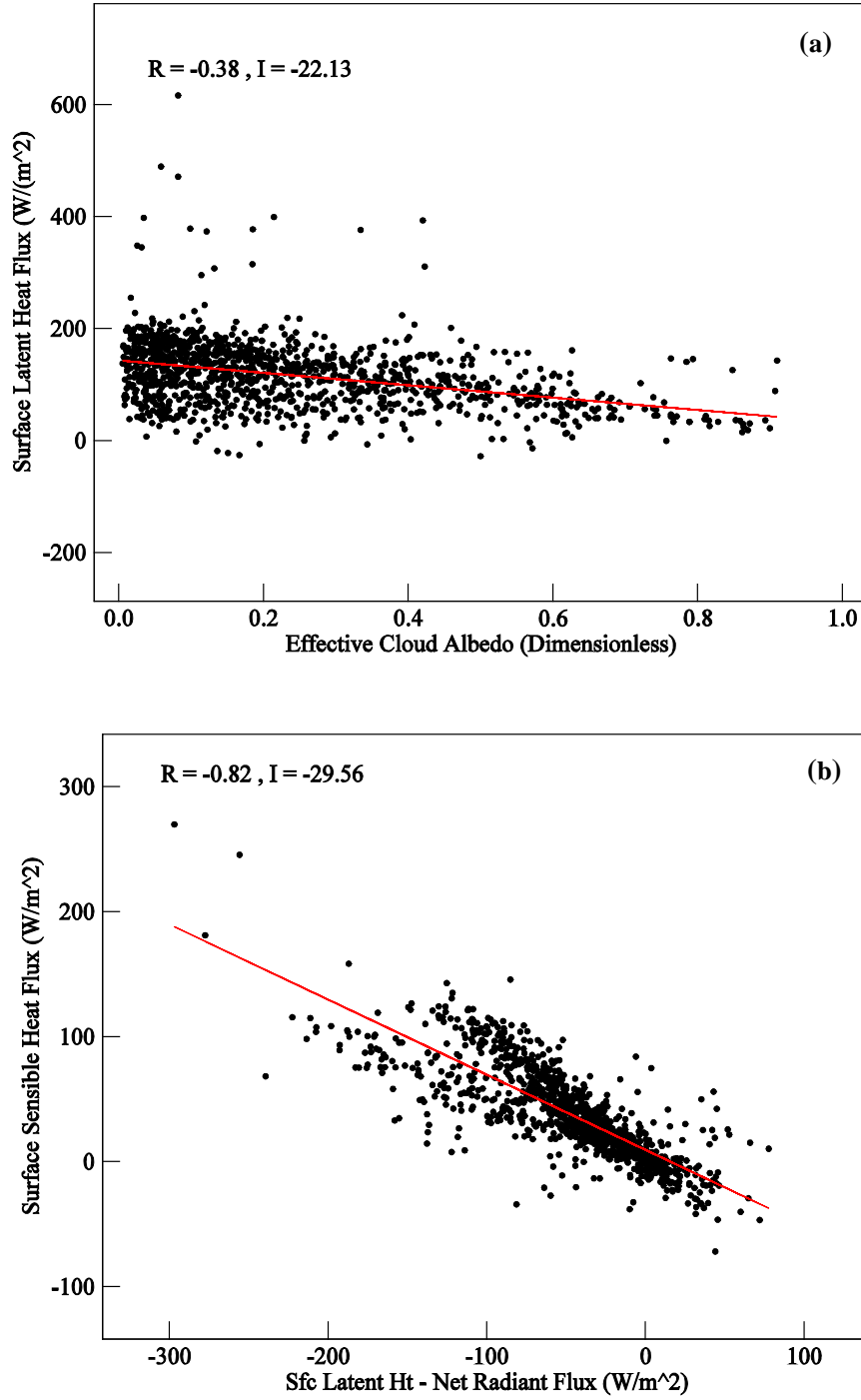


Figure 3: As in Figure 1, except for the surface latent heat flux  $LE$  (in  $W\ m^{-2}$ ) versus effective cloud albedo  $\alpha_c$  in (a) and the surface sensible heat flux  $H$  versus the difference  $LE - R_{net}$  of the surface latent heat flux and the net radiation (all in  $Wm^{-2}$ ) in (b).

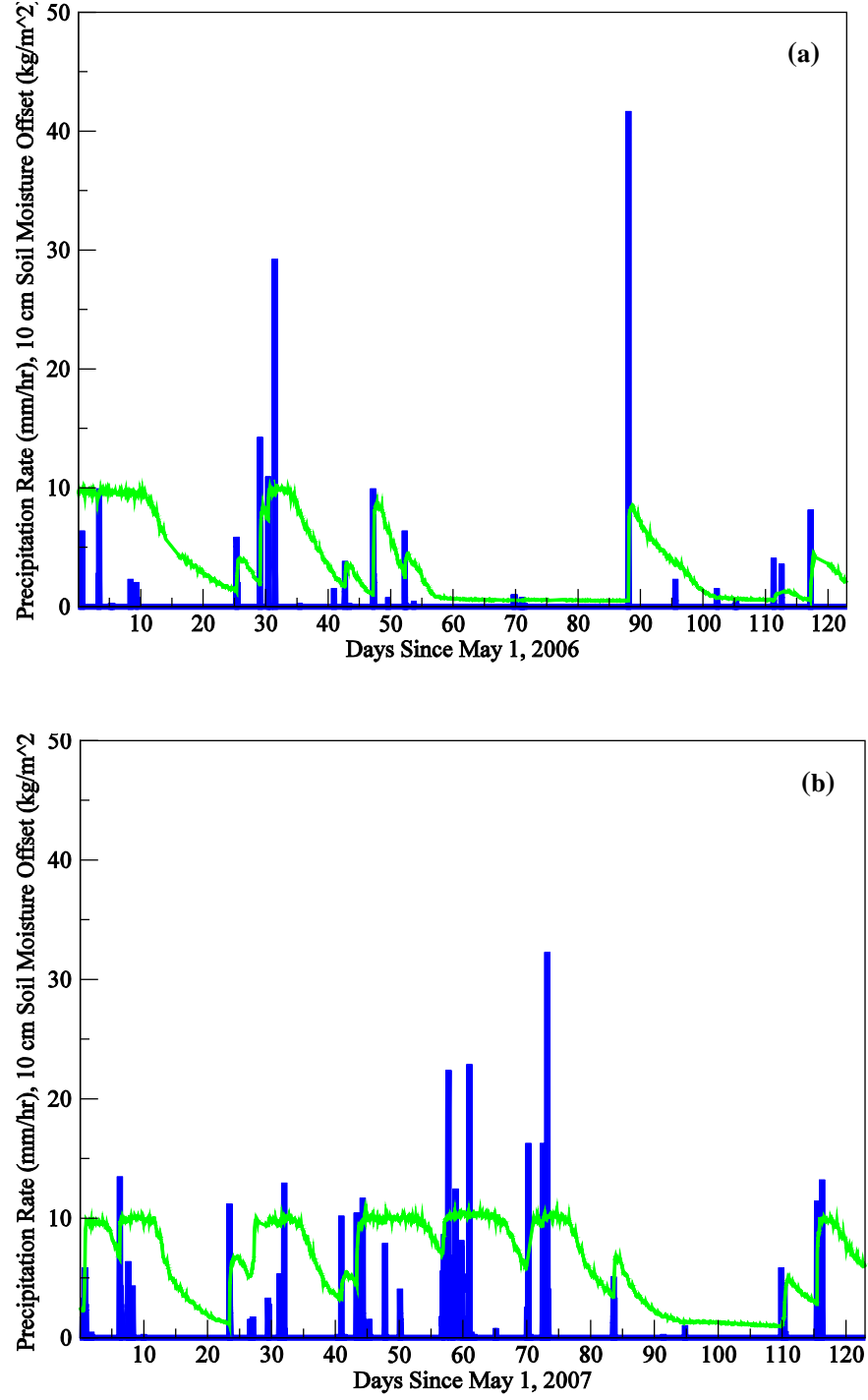


Figure 4: Warm-season hourly time series of SGP precipitation rate  $P$  (mm hr<sup>-1</sup> in blue ) versus soil moisture offset  $\Delta W = (W_{10cm} - 25)$  kg m<sup>-2</sup> for the top 10 cm of soil (in green) are shown for the anomalously dry year 2006 in (a), and for the anomalously wet year 2007 in (b).

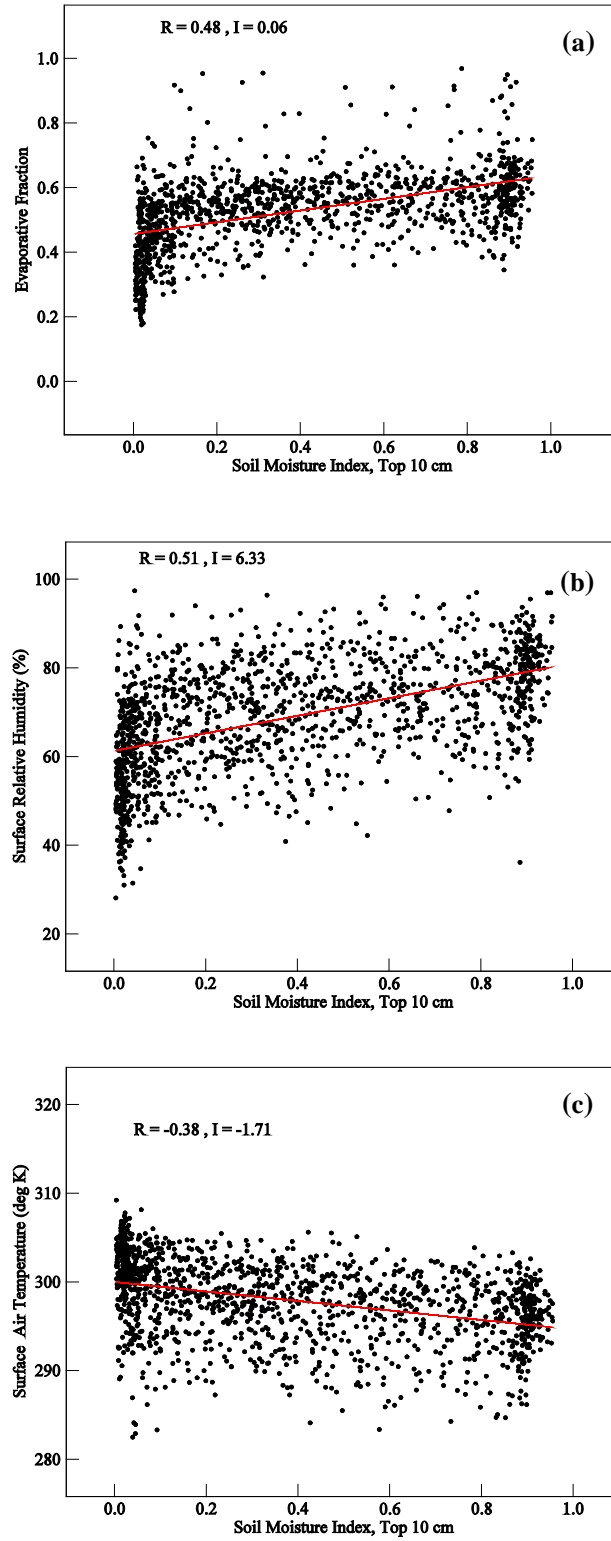


Figure 5: As in Figure 1, except for the surface evaporative fraction  $EF$  in (a), the surface relative humidity  $RH$  in (b), and the surface air temperature  $T_a$  in (c), all with respect to the 10-cm soil moisture index  $SMI_{10cm}$ .

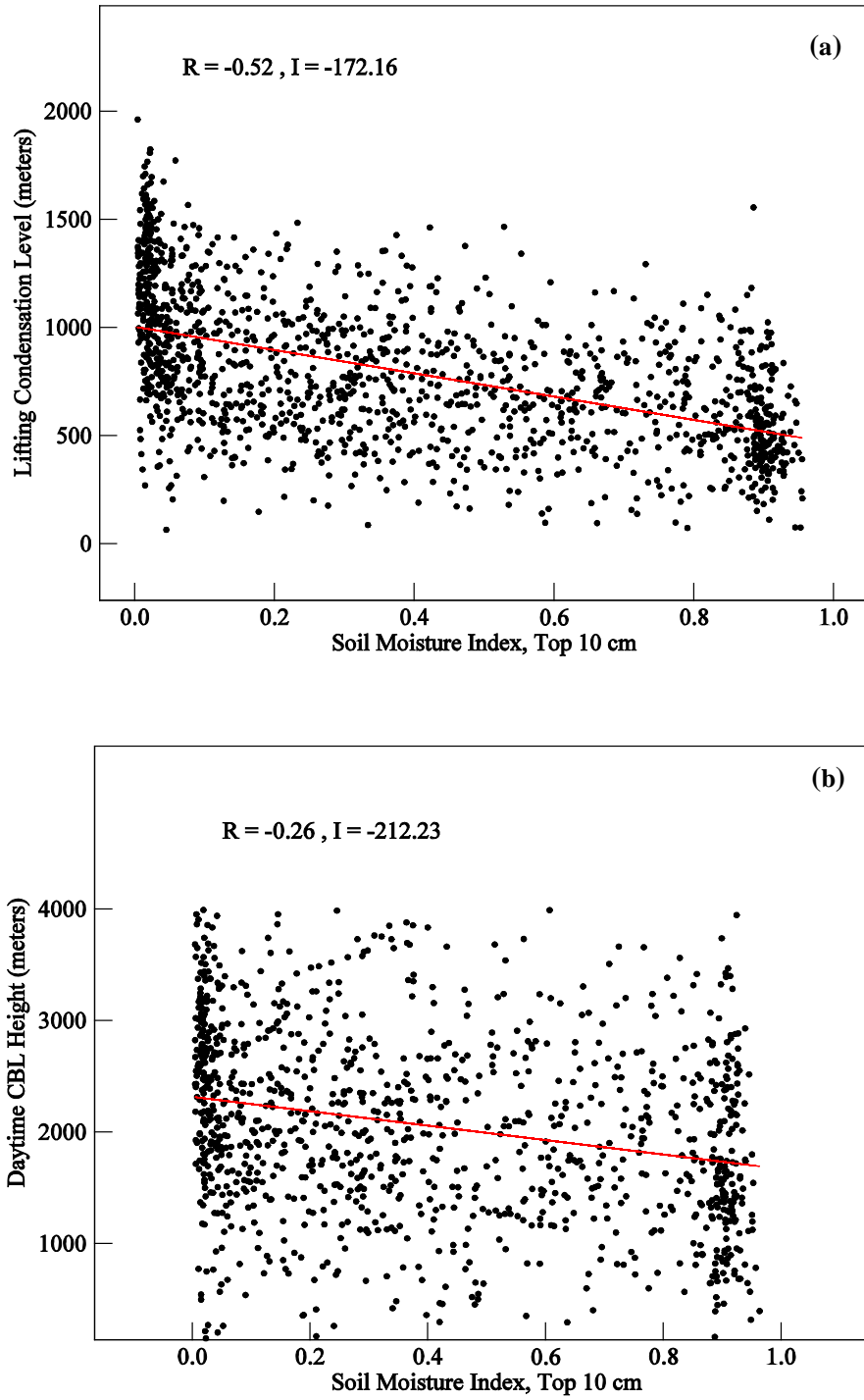


Figure 6: As in Figure 1, except for the derived lifting condensation level  $LCL$  (in meters) in (a), and the observed daytime-average cloud base level  $CBL$  for those clouds with bases below 4 km in (b), both with respect to the 10-cm soil moisture index  $SMI_{10cm}$ .

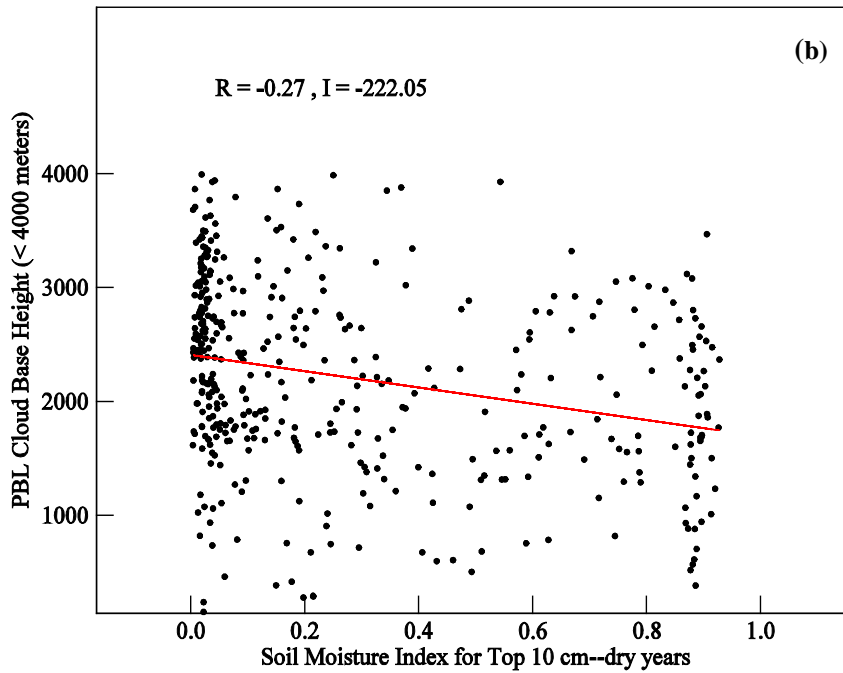
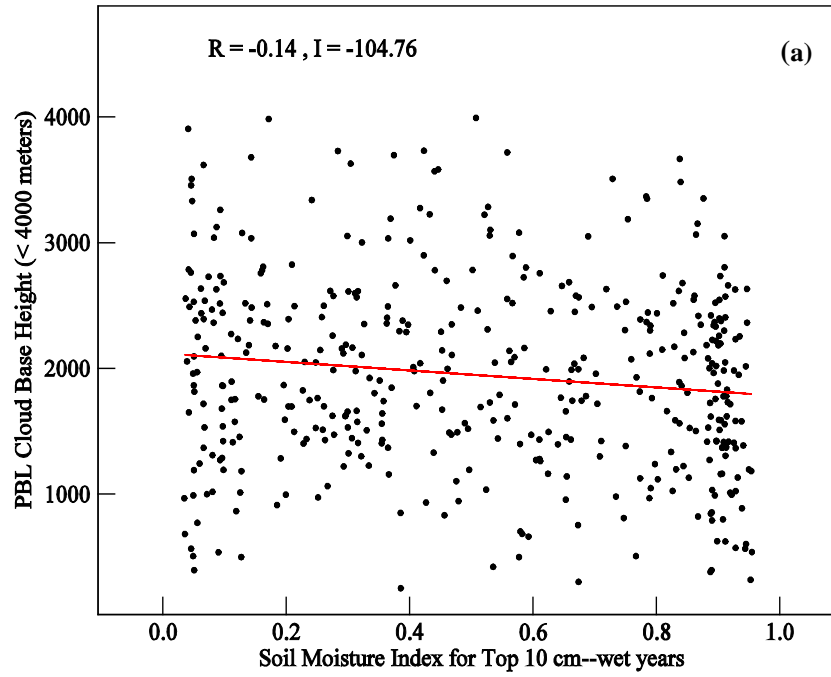


Figure 7: As in Figure 1, except for the observed cloud base level *CBL* for those clouds with bases below 4 km versus the 10-cm soil moisture index  $SMI_{10cm}$  for (a) the wet warm seasons of 2002,2004, 2007,and 2008, and (b) for the dry warm seasons of 1998, 2003, 2005, and 2006.

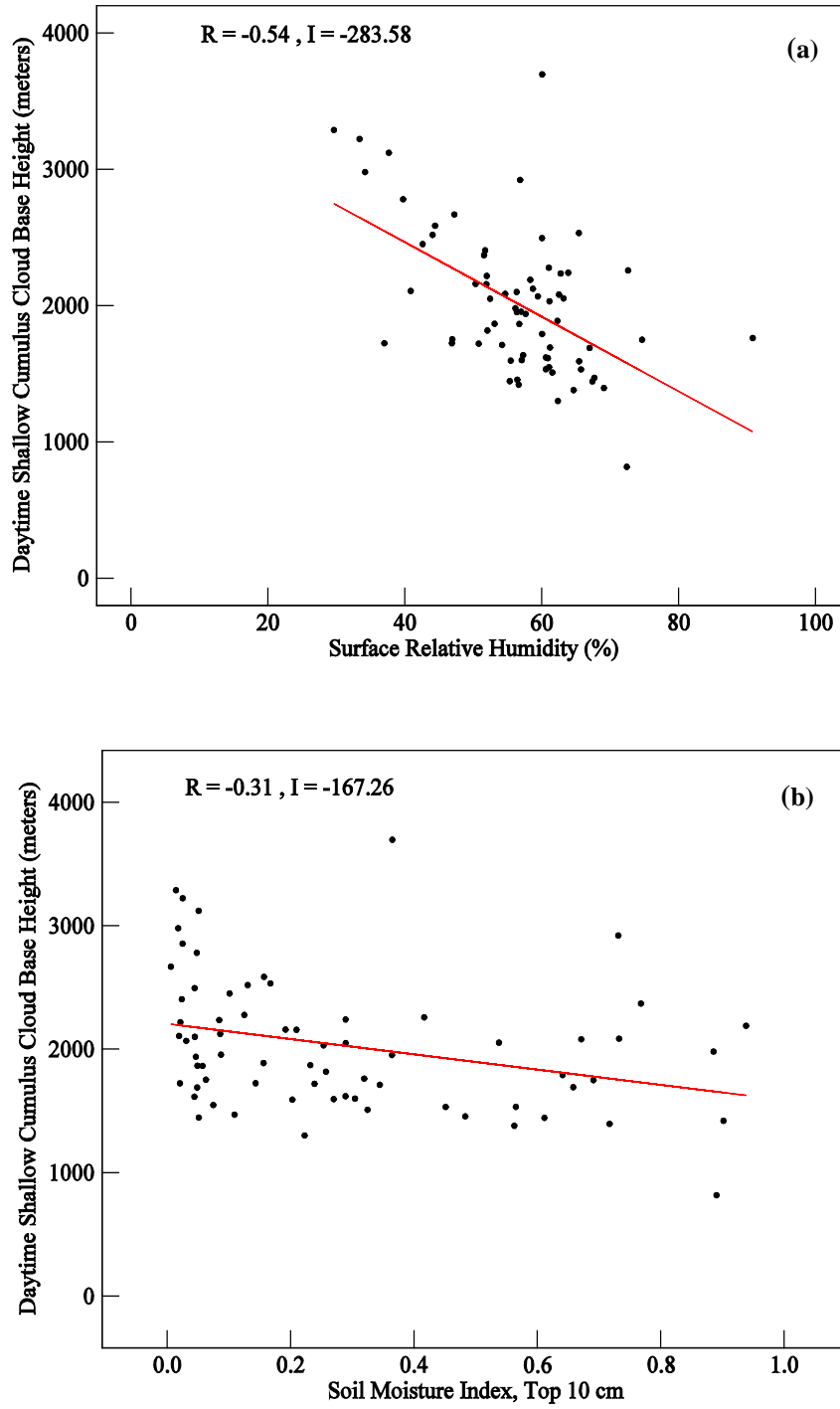


Figure 8: As in Figure 1, except for the observed daytime-average cloud base level  $CBL$  during occurrences of forced ("thin") or active ("thick") shallow cumulus clouds versus surface relative humidity  $RH$  in (a), and versus the 10-cm soil moisture index  $SMI_{10cm}$  in (b). See the text for further details.